Joule

Article

Carboxyl-functionalized perovskite enables ALD growth of a compact and uniform ion migration barrier

Graphical abstract

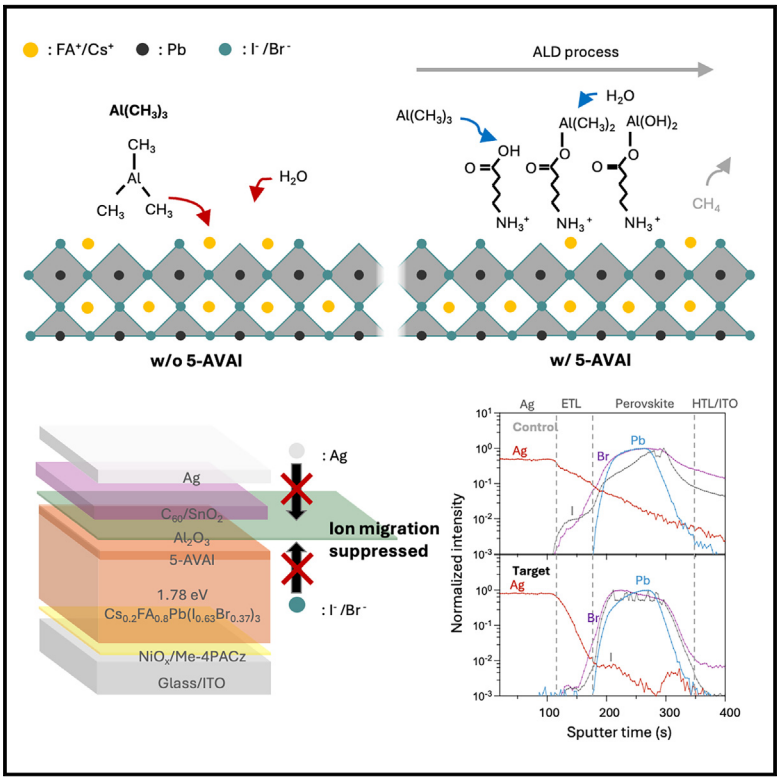

Highlights

- 5-AVAI facilitates high-quality ALD growth, preventing perovskite surface degradation
- 5-AVAI improves ALD-Al_2O_3 uniformity and suppresses ion migration
- The improved ALD-Al_2O_3 enables 1,000 h (at 55°C) operation with 90% PCE retention for 1.78 eV perovskite solar cells

Authors

Deokjae Choi, Donghoon Shin, Chongwen Li, ..., Nicholas Rolston, Edward H. Sargent, Bin Chen

Correspondence

ted.sargent@northwestern.edu (E.H.S.), bin.chen@northwestern.edu (B.C.)

In brief

We demonstrate a method to enhance the stability and efficiency of perovskite solar cells by developing a robust ion migration barrier using atomic layer deposition (ALD) of aluminum oxide (Al_2O_3). This is achieved by treating the perovskite surface with 5-ammonium valeric acid iodide (5-AVAI) to promote ALD growth. This approach improves the power conversion efficiency and longevity of cells, with 1.78 eV mixed-halide wide-band-gap devices retaining 90% initial efficiency after 1,000 h of maximum power point tracking at 55°C.

Choi et al., 2025, Joule 9, 101801
February 19, 2025
https://doi.org/10.1016/j.joule.2024.12.002

CellPress

Please cite this article in press as: Choi et al., Carboxyl-functionalized perovskite enables ALD growth of a compact and uniform ion migration barrier, Joule (2024), https://doi.org/10.1016/j.joule.2024.12.002

Joule

CellPress

Article

Carboxyl-functionalized perovskite enables ALD growth of a compact and uniform ion migration barrier

Deokjae Choi,[1,5] Donghoon Shin,[1,5] Chongwen Li,[1,5] Yuan Liu,[2,5] Abdulaziz S.R. Bati,[1,5] Dana E. Kachman,[2] Yi Yang,[1] Jiachen Li,[1] Yoon Jung Lee,[1] Muzhi Li,[3] Saivineeth Penukula,[3] Da Bin Kim,[4] Heejong Shin,[1] Chiung-Han Chen,[1] So Min Park,[1,6] Cheng Liu,[1] Aidan Maxwell,[4] Haoyue Wan,[1,4] Nicholas Rolston,[3] Edward H. Sargent,[1,2,4,*] and Bin Chen[1,7,*]

[1]Department of Chemistry, Northwestern University, Evanston, IL 60208, USA

[2]Department of Electrical and Computer Engineering, Northwestern University, Evanston, IL 60208, USA

[3]Renewable Energy Materials and Devices Laboratory, School of Electrical, Computer and Energy Engineering (ECEE), Arizona State University, 7700 S River Pkwy., Tempe, AZ 85284, USA

[4]Department of Electrical and Computer Engineering, University of Toronto, Toronto, ON M5S 3G4, Canada

[5]These authors contributed equally

[6]Present address: Department of Chemistry, National University of Singapore, Singapore 117543, Singapore

[7]Lead contact

*Correspondence: ted.sargent@northwestern.edu (E.H.S.), bin.chen@northwestern.edu (B.C.)

https://doi.org/10.1016/j.joule.2024.12.002

CONTEXT & SCALE Ensuring the stability of perovskite solar cells (PSCs) is essential to unlocking their potential as a high-efficiency solar technology. This research addresses a significant challenge in the field of PSCs: ion migration, which deteriorates the performance and stability of PSCs. By functionalizing the perovskite surface with 5-ammonium valeric acid iodide (5-AVAI), this study presents an approach for depositing high-quality aluminum oxide (Al_2O_3) on top via atomic layer deposition (ALD) at 100°C. The resulting compact and uniform Al_2O_3 layer acts as an effective ion migration barrier, significantly enhancing both the stability and power conversion efficiency of PSCs.

The implications of this study are relevant to the future commercialization of perovskite solar cells. ALD is already widely used in the industry for its ability to form uniform metal oxide layers over large areas, making the proposed method well suited for rapid adoption. Moreover, the ability to deposit metal oxides directly onto the perovskite surface without causing damage could open the door to inverted PSCs using inorganic electron transport layers, paving the way for the development of longer-lasting perovskite solar cells. This research marks an important step toward the practical application of perovskite solar technology.

SUMMARY

Mixed-halide wide-band-gap perovskites are critical components of highly efficient tandem cells, but their operating stability is limited by halide migration. Metal oxides deposited via atomic layer deposition (ALD) have been shown to block halide migration; however, previously pursued methods result in inhomogeneous nucleation and growth. We hypothesized that functionalizing the perovskite surface with ALD-active carboxyl groups could promote nucleation and enable higher-temperature metal oxide growth. We find that 5-ammonium valeric acid iodide (5-AVAI) facilitates the formation of a compact and uniform aluminum oxide (Al_2O_3) layer and allows growth at 100°C compared with the previous limit of 75°C. We demonstrate that halide migration into the C_{60} electron transport layer is reduced by a factor of 10 compared with the reference case. Al_2O_3-capped perovskite solar cells with a band gap of 1.78 eV retain 90% of their initial power conversion efficiency after 1,000 h of continuous operation under 1-sun illumination at 55°C.

INTRODUCTION

Band-gap tuning in metal halide perovskites enables tandem devices to have power conversion efficiencies (PCEs) higher than those of single-junction solar cells.[1,2] The field has shown remarkable progress, including that in certified PCE and operating stability, yet there remains room for improvement on the path to meeting the full suite of

Please cite this article in press as: Choi et al., Carboxyl-functionalized perovskite enables ALD growth of a compact and uniform ion migration barrier, Joule (2024), https://doi.org/10.1016/j.joule.2024.12.002

International Electrotechnical Commission (IEC) accelerated lifetime tests.

State-of-art all-perovskite tandem solar cells are made in a *p-i-n* architecture, with fullerene derivatives such as C_{60} and phenyl-C61-butyric acid methyl ester (PCBM) serving as the electron charge transport layer (ETL). Unfortunately, halides from the perovskite lattice have widely been observed to migrate into the fullerene-derivative layers.[3] These mobile ions lead to local charge accumulation and the formation of I^0 and Pb^0 defects, and these reduce the conductivity of the fullerene derivatives.[3,4] The migrated ions further travel to the metal electrodes, corroding these to form resistive layers that are barriers to efficient charge extraction.[5,6] These processes worsen over time, militating against the operating stability of all-perovskite tandem solar cells.[7,8]

Strategies have been proposed to passivate interface defects—the main ion migration pathways—based on spin-coating passivation agents such as organohalides,[9–11] Lewis bases,[12] and dipolar compounds.[13,14] These strategies have improved solar cell PCE, and yet ion migration persists at the perovskite/ETL interface.[5]

Depositing metal oxides on PSCs using atomic layer deposition (ALD) is a promising technique to improve solar cell durability. When metal oxide layers are compact and conformal, this prevents perovskite decomposition caused by the penetration of atmospheric elements such as moisture[15–17] and can potentially prevent detrimental interfacial ion migration. ALD-SnO_2 on C_{60} has been used to suppress ion migration into metal electrodes; however, to date, it has yet to completely prevent halides from diffusing into the ETL.[5]

During the deposition of metal oxides directly on top of a perovskite top surface,[18] the direct exposure of the perovskite layer to reactive precursors and oxidants used in ALD leads to the decomposition of organic cations in perovskites and the formation of PbI_2 residue.[19] The decomposition is further accelerated at higher processing temperatures; however, processing temperatures in the ~100°C range appear to be essential for achieving uniform and high-quality metal oxide layers.[20–22] For this reason, ALD metal oxide deposition on perovskites is typically performed at low temperatures, usually below 75°C (Table S1).

Here, we explore the introduction of protective layers onto the perovskites to simultaneously passivate the interface, promote the seeding of the metal oxide, and suppress ALD-induced degradation. We find that prior passivation agents do not protect the perovskite surface during ALD, for they do not withstand the 100°C processing temperature.

We hypothesize that the instability of these surface treatment ligands during ALD arises from a lack of active ALD sites, which results in poor nucleation of the metal oxide. This inadequate seeding causes non-uniform growth with voids through which the passivation agents desorb at 100°C.

To address this, we explore the use of a carboxyl-ammonium molecule, where carboxyl provides ALD-active sites for Al–O bonding, thereby mitigating the inhomogeneity-induced instability. We used 5-ammonium valeric acid iodide (5-AVAI) to functionalize the perovskite surface with carboxyl (–COOH) groups that preferentially bind with ALD precursors during aluminum oxide (Al_2O_3) deposition.[23,24] We found that 5-AVAI enables a uniform Al_2O_3 film on the perovskite and prevents degradation, confirmed by photoluminescence (PL) mapping and kelvin probe force microscopy (KPFM). This resulted in a more compact and robust barrier layer against ion migration, leading to improved solar cell stability: an encapsulated wide-band-gap (WBG) solar cell retained 99% of initial PCE in ambient air under maximum power point (MPP) tracking under 1-sun illumination at 25°C for 615 h. Subsequently, the same device retained 90% of its maximum PCE during aging under 1-sun illumination at 55°C over 1,000 h.

RESULTS AND DISCUSSION

ALD-Al_2O_3 growth on the perovskite surface with different passivation ligands

We first deposited ALD-Al_2O_3 on perovskite films using chamber temperatures ranging between 60°C and 100°C and measured X-ray diffraction (XRD) spectra (Figure S1). For the layer deposited at 100°C, a PbI_2 peak was observed upon Al_2O_3 deposition. ALD precursors (trimethyl aluminum [TMA]) and/or the oxidant (deionized [DI] water) damage the perovskite films during the deposition process (Figure 1A). The PbI_2 peak diminished as the ALD temperature decreased, which indicates that the degradation can be alleviated by reducing the process temperature, as this reduces the reactivity of the precursor and oxidant.[8,18–20] However, the reduction in reaction temperature could also lead to decreased uniformity of the Al_2O_3 layer due to less reactivity.[20,22] This motivated us to seek to stabilize the perovskite surface to avoid decomposition during the ALD process at higher temperatures.

We investigated previously reported passivation ligands to protect against the ALD process chemistry (Figure S2). We chose phenethylammonium iodide (PEAI) and n-butylammonium iodide (BAI) as representative 2D cations employed in fabricating 2D/3D perovskites. These passivation ligands have an ammonium ($–NH_3^+$) group anchoring to the perovskite surface and another functional group (e.g., benzene and methyl) that extends away from the perovskite surface.[24] Figure 1B shows XRD spectra of the control film and the perovskite films with passivation ligands before and after Al_2O_3 deposition. We observed the PbI_2 peak emerging after Al_2O_3 deposition for films with PEAI and BAI treatment, indicating that they cannot protect the perovskite films during the ALD process (Figures 1B and S3).[22]

Time-of-flight secondary ion mass spectroscopy (ToF-SIMS) was used to analyze the presence of passivation ligands on the perovskite surface before and after Al_2O_3 deposition (Figure 1C). However, PEA^+ and BA^+ could not be found on perovskite films after Al_2O_3 deposition. We believe that that PEA^+ and BA^+ deprotonate at temperatures higher than 85°C and desorb from the perovskite surface during ALD.[25]

We sought to functionalize the perovskite surface to introduce favorable binding sites for precursor seeding and protect the perovskite from damage during ALD. Because ALD growth depends on the reaction between precursors and –OH groups on the substrate surface, we chose a carboxyl-ammonium ligand (5-AVAI). The ligand provides a carboxyl group to react with the TMA precursor for ALD Al_2O_3 growth while anchoring to

Please cite this article in press as: Choi et al., Carboxyl-functionalized perovskite enables ALD growth of a compact and uniform ion migration barrier, Joule (2024), https://doi.org/10.1016/j.joule.2024.12.002

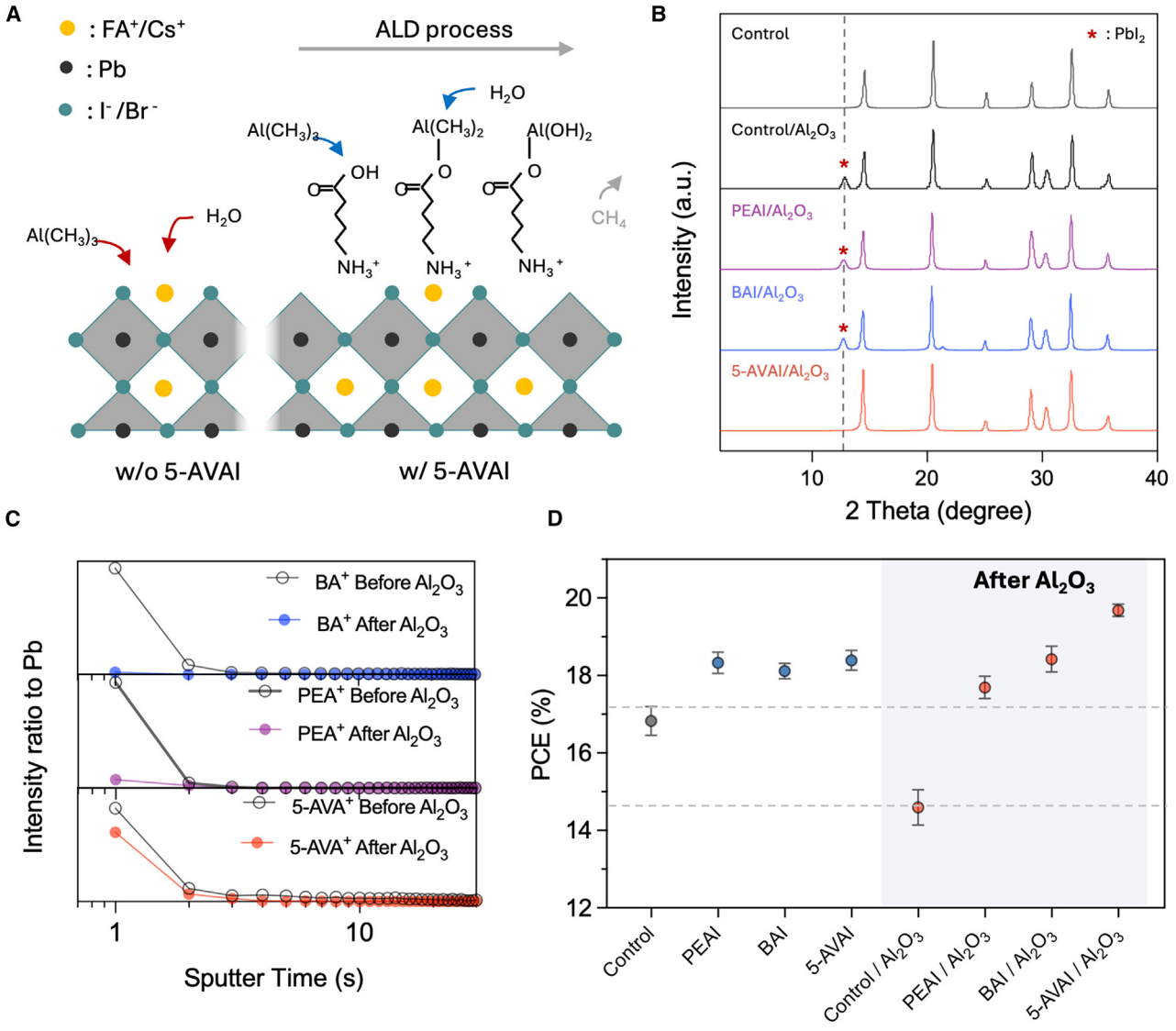

Figure 1. ALD-Al_2O_3 growth on the perovskite surface with different passivation ligands

(A) Schematic showing perovskite surface with passivation ligands exposed to trimethyl aluminum (TMA) and water during the Al_2O_3 deposition.

(B) XRD spectra of the control film and perovskite films with passivation ligands after Al_2O_3 deposition.

(C) ToF-SIMS spectra of passivation ligands on perovskite before and after Al_2O_3 deposition.

(D) PCEs of control versus passivated PCSs using different passivation ligands before and after Al_2O_3 deposition. Eight devices of each set of samples were measured.

the perovskite via the ammonium group, confirmed by contact angle measurement (Figure S4).[26–28] A previous study using molecular dynamics simulations also demonstrated that, for long chain ligands like 5-AVAI, the ammonium group preferentially anchors to the perovskite, with the carboxyl group pointing outward.[24] Films with 5-AVAI showed no observable PbI_2 peak after Al_2O_3 deposition (Figures 1B and S3) and we found that 5-AVA^+ survives the Al_2O_3 deposition at 100°C via ToF-SIMS measurement (Figure 1C). 5-AVAI appears thus to function as a buffer layer that prevents the perovskite from degradation during ALD at 100°C. The growth of Al_2O_3 via ALD occurs through the interaction between the methyl groups ($-CH_3$) in the TMA precursor and the carboxyl group. This interaction promotes the formation of strong Al–O bonds (Figures 1A and S5).[29–33] The chemical Al–O bonds may function as a capping layer to prevent 5-AVA^+ from escaping during the ALD process. The photovoltaic performance of PSCs after Al_2O_3 deposition on these passivation ligands is consistent with the XRD and ToF-SIMS results (Figure 1D). 5-AVAI treatment shows improvement in PCE with Al_2O_3 deposition. Other passivation ligands with Al_2O_3 showed lower performance, consistent with the observation of PbI_2 formation related to the ALD-Al_2O_3 process.

Please cite this article in press as: Choi et al., Carboxyl-functionalized perovskite enables ALD growth of a compact and uniform ion migration barrier, Joule (2024), https://doi.org/10.1016/j.joule.2024.12.002

To investigate the effect of the ligand carbon chain length on ALD growth, we tested three carboxyl-ammonium molecules of varying lengths—3-ammonium propionic acid iodide (3-APAI), 4-ammonium butyric acid iodide (4-ABAI), and 5-AVAI. XRD analysis showed that 3-APAI and 4-ABAI failed to fully protect the perovskite from decomposing into PbI_2 during ALD-Al_2O_3 deposition (Figure S6). In contrast, 5-AVAI successfully prevented degradation. This observation is consistent with molecular dynamics simulations reported in a previous study,[24] which showed that longer carbon chains promote the outward orientation of carboxyl groups on the perovskite surface. We did not pursue ligands with a longer chain than 5-AVAI as they could negatively impact charge carrier extraction.

Compact and uniform ALD-Al_2O_3 passivation for reducing nonradiative recombination at the perovskite/C_{60} interface

Notably, we found that 5-AVAI plays a key role in both ALD-oxide uniformity and the reduction of nonradiative recombination at the interface between the perovskite and C_{60}. To investigate the impact of interface defect passivation by ALD-Al_2O_3, we conducted photoluminescence quantum yield (PLQY) measurements. We found that Al_2O_3, 5-AVAI, and 5-AVAI/Al_2O_3 all offer surface chemical passivation, as shown by the improved PLQYs of perovskite films on quartz and hole transport layer (HTL) substrates (Figure 2A). The control perovskite film exhibits a drop in PLQY of nearly 2 orders of magnitude upon the addition of C_{60} (full stack), and each post-treatment significantly reduces the magnitude of these losses. In particular, 5-AVAI/Al_2O_3 retains the highest level of PLQY in the full stack. Time-resolved photoluminescence (TRPL) results of films on glass substrates show enhanced carrier lifetimes for films after treatment, indicating reduced nonradiative recombination (Figure 2B; Table S2). The carrier lifetimes of the control, Al_2O_3, 5-AVAI, and 5-AVAI/Al_2O_3 were 16.9, 12.8, 39.4, and 122.7 ns, respectively. Both PLQY and TRPL suggest that the incorporation of the 5-AVAI/Al_2O_3 film yields a less defective surface compared with the control and Al_2O_3 films.

We investigated ALD-Al_2O_3 thickness and uniformity. The thickness of 10-cycle ALD-Al_2O_3 on the Si substrate was measured to be 1.1 nm using an ellipsometer and a profilometer (Figure S7). The millimeter-scale photoluminescence (PL) intensity distribution of the perovskite films was conducted to investigate the uniformity of Al_2O_3 deposition on the perovskite surface before and after 5-AVAI treatment (Figures 2C–2E and S8). Compared with the control film, there are localized areas where the PL intensity is enhanced after Al_2O_3 deposition without 5-AVAI treatment. Conversely, the overall PL intensity of the 5-AVAI/Al_2O_3 film is not only improved but the distribution is also more uniform, suggesting that 5-AVAI facilitates the uniform deposition of the Al_2O_3 layer on the perovskite film. This is consistent with the KPFM images (Figures 2F–2H), which demonstrate that 5-AVAI/Al_2O_3 has narrower potential distribution (3.60 mV compared with 5.17 mV for the control). Consequently, the improved uniformity of Al_2O_3, facilitated by the –COOH ALD-active sites in the 5-AVAI layer, significantly reduces the direct contact between C_{60} and the perovskite. This leads to the suppression of nonradiative recombination, in agreement with the PLQY and TRPL results.[34]

Performance and stability of WBG perovskite solar cells

We then fabricated single-junction WBG perovskite solar cells with a band gap of 1.78 eV (Figure 3A). We used the device structure indium tin oxide (ITO)/NiO_x/[4-(3,6-dimethyl-9H-carbazol-9-yl)butyl]phosphonic acid (Me-4PACz)/$Cs_{0.2}FA_{0.8}Pb(I_{0.63}Br_{0.37})_3$ perovskite/5-AVAI/ALD-Al_2O_3/C_{60}/ALD-SnO_2/Ag. Compared with the control device (1.24 V and 77.9%), the target device (1.31V and 83.1%) exhibited higher V_{OC} and FF (Figures 3B and 3C). The narrower distribution of V_{OC} and FF in the target device compared with the control (Figure 3C) can be attributed to the uniform post-treatment, as evidenced by the improved uniformity (Figures 2C–2E and S8). The short-circuit current density (J_{SC}) and 1.78 eV of band gap were confirmed with external quantum efficiency (EQE) measurement in Figure S9.

We found that ALD-Al_2O_3, assisted by 5-AVAI, suppressed ion migration throughout the devices. We tracked the ion migration in control and target devices via ToF-SIMS after 85°C aging at open circuit conditions under 1-sun illumination for 72 h (Figure 3D). Control devices (ITO/NiO_x/Me-4PACz/$Cs_{0.2}FA_{0.8}Pb(I_{0.63}Br_{0.37})_3$ perovskite/C_{60}/ALD-SnO_2/Ag exhibit Ag ions that have migrated to the perovskite layer. Halide anions, such as I and Br ions, migrated from the perovskite layer to ETL and electrodes. The bromide ion has a smaller size and higher diffusivity than does iodide, consistent with the poor stability performance in WBG devices.[5] However, after Al_2O_3 deposition on the control film, the ion migration was suppressed (Figure S10). When we deposited Al_2O_3 on the 5-AVAI-treated perovskite (target device), ion migration is even further suppressed. Compared with the control device, the target device shows 1 order magnitude fewer ions, including Ag, I, and Br, at the interface between ETL and the perovskite. This we attribute to a more uniform and compact Al_2O_3 layer protecting against ion migration, as confirmed in Figure 2.

The reduction in ion migration into the ETL minimizes overall ion migration within the film and toward the HTL, as the decreased number of halide ions migrated into ETL reduces halide vacancies in the bulk—the vehicle for ion migration.[35] This suppression of ion migration is further confirmed by comparing the mobile ion concentration (N_o) of control and target devices using a transient dark current measurement (Figure S11).[4] At room temperature, the control device shows a N_o of 3.1×10^{14} cm^{-3} whereas the target device shows a lower N_o of 5.5×10^{13} cm^{-3}. At ~70°C—the highest temperature tested for the devices in this work—the target device shows a N_o of 2.9×10^{14} cm^{-3}, markedly lower than the N_o of 7.2×10^{14} cm^{-3} of the control device. This indicates that ALD-Al_2O_3 suppresses ion migration at higher temperatures. This trend observed in N_o holds even after the devices are aged. Additionally, the control device exhibits an activation energy (E_A) of 0.12 eV whereas the target device exhibits a higher E_A of 0.14 eV, and the control device exhibits an order-of-magnitude-higher ionic conductivity in comparison with the target device, both before and after aging (Figure S12). Higher E_A and lower ionic conductivity indicate that ion migration is suppressed in terms of ion formation and movement, respectively. We also investigated the ion migration behavior in target devices depending on different ALD processing temperatures. Higher-temperature-processed devices show

Please cite this article in press as: Choi et al., Carboxyl-functionalized perovskite enables ALD growth of a compact and uniform ion migration barrier, Joule (2024), https://doi.org/10.1016/j.joule.2024.12.002

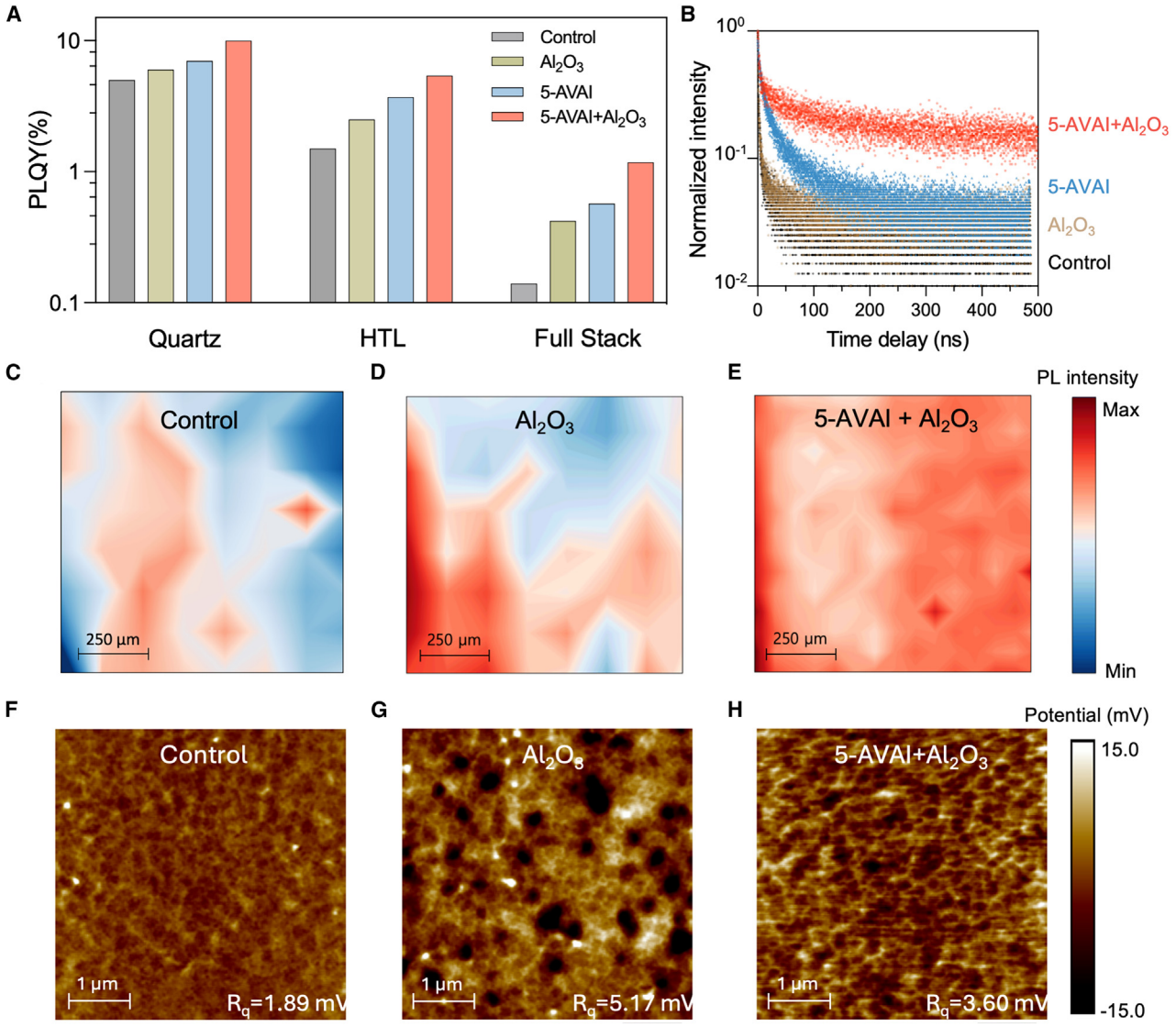

Figure 2. Uniform ALD-Al_2O_3 passivation for reducing nonradiative recombination at the perovskite/C_{60} interface

(A) PLQY of control (untreated), Al_2O_3, 5-AVAI, and 5-AVAI + Al_2O_3 films on quartz and HTL (NiO_x and Me-4PACz) substrates, as well as full device stacks (HTL/perovskite/C_{60}).

(B) Transient photoluminescence traces for the control, Al_2O_3, 5-AVAI, and 5-AVAI + Al_2O_3 films on glass substrates.

(C–E) The PL intensity distribution of 1 mm^2 perovskite films of (C) control, (D) Al_2O_3, and (E) 5-AVAI+Al_2O_3.

(F–H) Kelvin probe force microscopy of perovskite films of (F) control, (G) Al_2O_3, and (H) 5-AVAI+Al_2O_3.

suppressed ion migration, an observation we connect with a more uniform Al_2O_3 deposition at higher temperatures (Figures S13 and S14).

The suppressed ion migration results in WBG PSCs retaining 99% of initial efficiency, tracked under continuous 1-sun illumination at the MPP at 25°C over 615 h. For the same device, we then proceeded to study operating stability at MPP at 55°C. It retains 90% of its initial PCE following operation at MPP under 1-sun illumination over 1,000 h. These stability results surpass other ambient air stability reports for encapsulated WBG PSCs having E_g 1.78 ± 0.02 eV (Table S3).

All-perovskite tandem solar cells

We then incorporated our WBG active layer into monolithic all-perovskite tandem solar cells in combination with a $Cs_{0.05}FA_{0.7}MA_{0.25}Pb_{0.5}Sn_{0.5}I_3$ of ~1.2 eV NBG perovskite. The tandem device structure is ITO/NiO_x/Me-4PACz/WBG perovskite/5-AVAI/ALD-Al_2O_3/C_{60}/ALD-SnO_x/Au 1 nm/poly(3,4-ethylenedioxythiophene) polystyrene sulfonate (PEDOT:PSS)/NBG perovskite/C_{60}/bathocuproine (BCP)/Ag (Figure 4A), with the scanning electron microscopy (SEM) image showing the stack of WBG and NBG devices (Figure 4B). *J-V* scans of champion WBG, NBG, and tandem devices are shown in

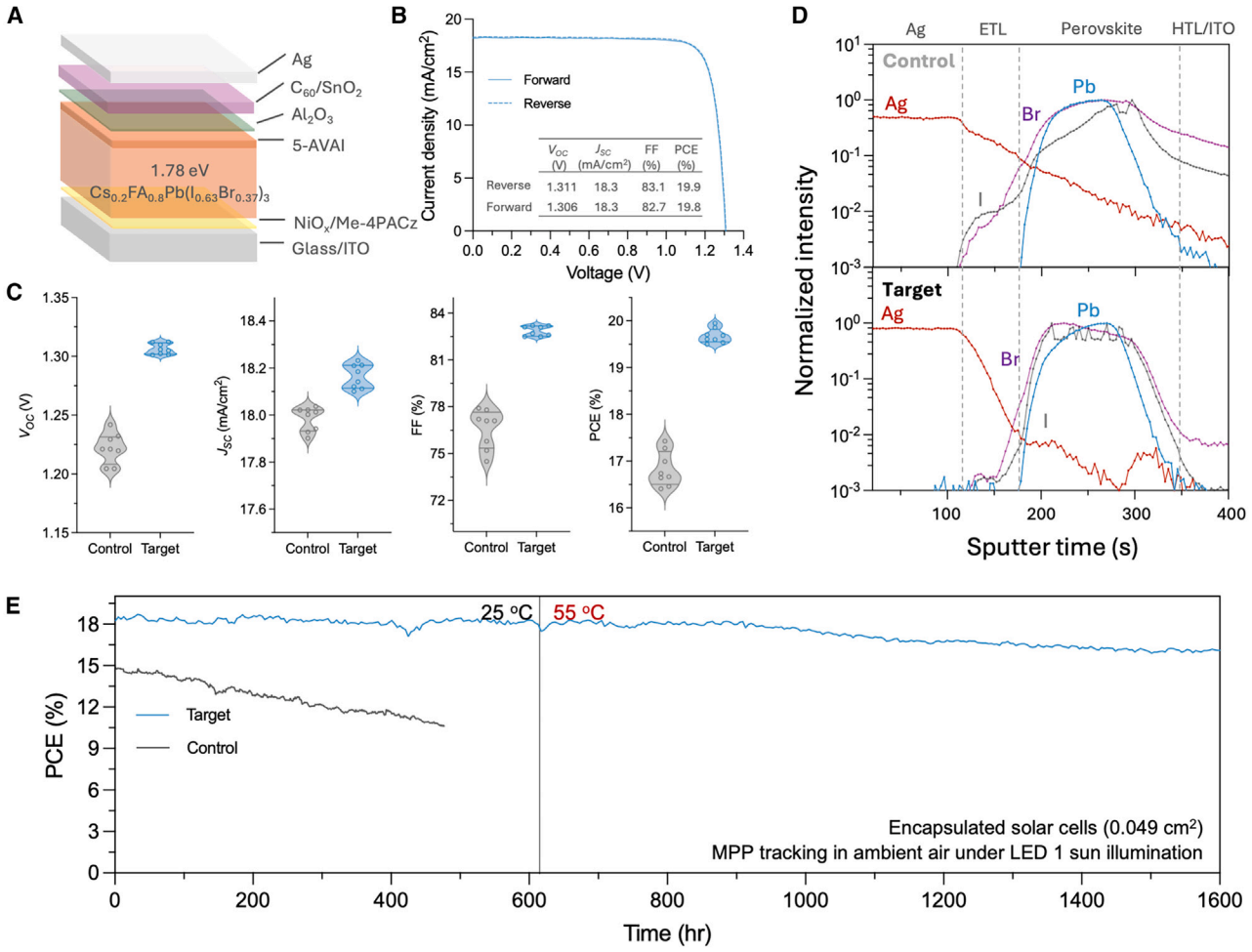

Figure 3. Characterization of WBG perovskite solar cells

(A) Schematic showing WBG device structure.

(B) *J-V* curves of PSCs with 5-AVAI and Al_2O_3 WBG devices.

(C) Histogram of V_{OC}, J_{SC}, FF, and PCE of control versus target for 8 devices. The device's active area was 0.049 cm^2.

(D) ToF-SIMS spectra of control and target device after open circuit aging at 85°C under 1-sun illumination for 72 h.

(E) Maximum power point (MPP) tracking of single-junction WBG devices under continuous AM 1.5G illumination. Devices were encapsulated, and MPP tracking was carried out under ambient air at 25°C for 615 h and subsequently at 55°C for 1,000 h conditions.

Figures 4C and S15. We report a PCE of 27.1% (with a stabilized power output of 26.7% in Figure 4D) with a V_{OC} of 2.11 V, along with a J_{SC} of 16.0 mA/cm^2 and an FF of 80.4%. From EQE measurements of each subcell, the integrated J_{SC} values of 15.5 and 15.2 mA/cm^2 were obtained, respectively. The calculated band gap of the WBG and NBG subcells from EQE spectra were 1.78 and 1.24 eV, respectively (Figure 4E). The tandems retain 90% of their initial PCE, limited by the NBG cell, after 500 h of continuous operation under AM 1.5G illumination (Figure 4F).

Conclusions

In summary, we present a strategy for depositing a compact and uniform ion migration barrier for PSCs to enhance both the device stability and efficiency. This is achieved by functionalizing the perovskite surface with carboxyl ligands (5-AVAI), which facilitates the formation of a uniform Al_2O_3 layer and prevents degradation during ALD deposition at 100°C. As a result, ALD-Al_2O_3 layers on carboxyl-functionalized perovskite are more resistant to ion migration, improving WBG solar cell stability and retaining 90% of its initial PCE after 1,000 h MPP tracking at 55°C under 1-sun illumination. We integrate the improved WBG perovskite into all-perovskite tandems with 27.1% of PCE, indicating relevance to the continued global effort to advance efficient, stable perovskite-based solar cells. We anticipate that the concept of an ALD-seeding layer using suitable molecular groups can be generalized to other metal oxides and perovskite systems. The ability to deposit ALD-based metal oxides directly onto the perovskite surface without causing damage could enable inverted PSCs using inorganic ETLs, paving the way for developing highly stable and durable perovskite solar cells.

Please cite this article in press as: Choi et al., Carboxyl-functionalized perovskite enables ALD growth of a compact and uniform ion migration barrier, Joule (2024), https://doi.org/10.1016/j.joule.2024.12.002

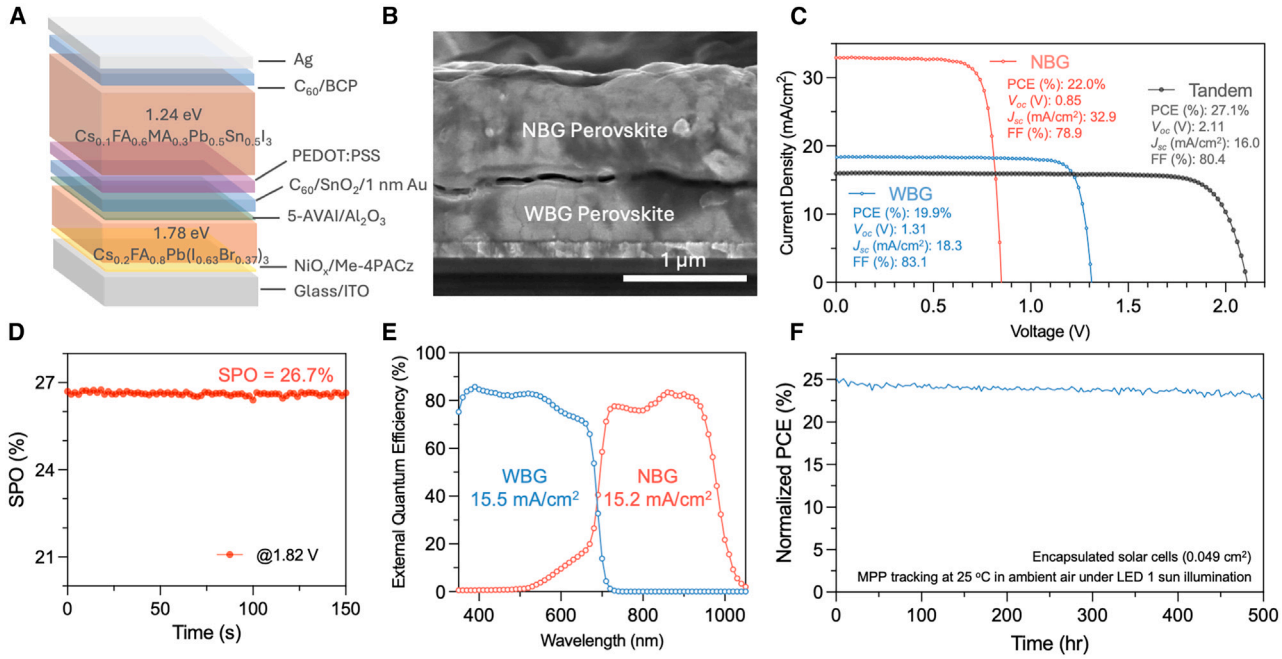

Figure 4. Monolithic all-perovskite tandem solar cells

(A) Schematic diagram of all-perovskite tandem device structure.

(B) Cross-sectional scanning electron microscopy (SEM) image of tandem device.

(C) *J-V* curves of the champion WBG, NBG, and tandem devices.

(D) Power output of the champion tandem device for 150 s exhibiting a stabilized PCE of 26.7%.

(E) EQE spectra of WBG and NBG subcells within the tandem devices.

(F) Maximum power point (MPP) tracking of single-junction WBG devices and all-perovskite tandems under continuous AM 1.5G illumination. Devices were encapsulated, and MPP tracking was carried out under ambient air at 25°C conditions.

EXPERIMENTAL PROCEDURES

Materials

All materials were used as received without further purification. Commercial ITO substrates (20 Ω/sq) with 25 mm × 25 mm dimensions were purchased from TFD. The organic halide salts, formamidinium iodide (FAI), methylammonium iodide (MAI), and formamidinium bromide (FABr), were purchased from GreatCell Solar Materials (Australia). PbI_2 (99.99%), $PbBr_2$ (99.999%), CsBr (>99.0%), and Me-4PACz were purchased from TCI Chemicals. CsI (99.999%) was purchased from Sigma-Aldrich. C_{60} and BCP were purchased from Xi'an Polymer Light Technology (China). All the solvents used in the process were anhydrous and purchased from Sigma-Aldrich. Tetrakis(dimethylamino) tin (iv) (99.9999%) for ALD SnO_2 source was purchased from STREM. PEDOT:PSS) aqueous solution (AI 4083) was purchased from Ossila. SnI_2 (99.99%), guanidine thiocyanate (GuaSCN, 99%), Sn powder, SnF_2 (99%), ethane-1,2-diammonium iodide (EDA), and glycine hydrochloride (GlyHCl) were purchased from Sigma-Aldrich. 3-APAI, 4-ABAI, and 5-AVAI were purchased from Greatcell Solar Materials.

Perovskite precursor solutions

WBG perovskite

1.05 M WBG perovskite precursor solution with a composition of $Cs_{0.2}FA_{0.8}Pb(I_{0.63}Br_{0.37})_3$ was prepared by dissolving CsI, CsBr, FAI, FABr, $PbBr_2$, and PbI_2 in mixed solvents of dimethylformamide (DMF) and dimethyl sulfoxide (DMSO) with a volume ratio of 4:1. The precursor solution was stirred at 60°C for 1 h and then filtered using a 0.22-μm polytetrafluoroethylene (PTFE) membrane before use.

Narrow-band-gap perovskite

1.8 M narrow-band-gap perovskite precursor solution with a composition of $Cs_{0.1}FA_{0.6}MA_{0.3}Pb_{0.5}Sn_{0.5}I_3$ was prepared by dissolving CsI, FAI, MAI, SnI_2, and PbI_2 in the mixed solvents of DMF and DMSO with a volume ratio of 3:1. Additives, including tin powders (5 mg/mL), GuaSCN (4 mg/mL), SnF_2 (14 mg/mL), and GlyHCl (4 mg/mL), were added to the precursor solution. The precursor solution was stirred for 1 h at 45°C and then filtered using a 0.22-μm PTFE membrane before use.

Solar cell fabrication

Single-junction WBG perovskite solar cell

NiO_x nanoparticle solution (purchased from Avantama) layer was first spin-coated on ITO substrates at 4,000 rpm for 25 s in the air without any post-treatment, and then the substrates were immediately transferred to the glovebox. NiO_x solution was diluted using ethanol with a ratio of 10:1. Me-4PACz (0.3 mg/mL) in ethanol was spin-coated on the NiO_x film at 4,000 rpm for 25 s and then annealed at 100°C for 10 min. For the perovskite film fabrication, the substrate was spun at 4,000 rpm for 32 s with an acceleration of 1,000 rpm; 100 μL Anisole was dropped onto the substrate during the last 10 s of the spinning. The substrates were then transferred onto a hotplate and heated at 100°C for 15 min. The surface treatment was finished by depositing 100 μL of 5-AVAI solution (1 mg/mL in IPA) onto the perovskite film surface at a spin rate of 4,000 rpm for 25 s with a 1,000-rpm/s acceleration. The film was then annealed at 100°C for 5 min. After cooling down to room temperature, the substrates were then transferred to the ALD system (Arradiance) to deposit 10 cycles of Al_2O_3 at 100°C using precursors of TMA and DI water. The pulse and purge time of TMA is 60 ms and 50 s with a 40-sccm of N_2 flow. The pulse and purge time of DI water is 60 ms and 50 s with a 40-sccm of N_2 flow. The substrates were transferred to the evaporation system, and 27-nm-thick C_{60} film was subsequently deposited on top by thermal evaporation at a rate of 0.2 Å/s. The substrates were then transferred to the ALD system (Savaanah) to deposit 15 nm SnO_2 at 100°C using precursors of tetrakis(dimethylamino) tin (iv) (99.9999%) and DI water. The pulse and purge time of Sn is 0.5 s and 15 s with a 20-sccm of N_2 flow. The pulse and purge time of DI water is

15 ms and 15 s with a 20-sccm of N_2 flow. A 140-nm Ag electrode was then deposited by thermal evaporation at a rate of 1 Å/s.

All-perovskite tandem solar cells

The WBG perovskite solar cell fabrication was completed as described above until the deposition of ALD-SnO_2. After the ALD deposition of SnO_2, 1 nm of Au was deposited by thermal evaporation. Next, PEDOT:PSS (diluted at a 1:2 volume ratio in IPA) was spin-coated onto the WBG subcell at 4,000 rpm for 30 s and then annealed at 120°C for 10 min in the air. After cooling, the substrates were transferred to a nitrogen-filled glovebox for the deposition of the NBG subcell. The NBG perovskite precursor solution was spin-coated onto the substrates at 1,000 rpm for 10 s, followed by 3,800 rpm for 45 s. During the second spin-coating step, 400 μL of toluene was poured onto the substrate 20 s before the end. The substrate was then annealed at 100°C for 10 min. Post-treatment with EDA was carried out by spin-coating a solution of 1 μL EDA in 20 ml of chlorobenzene (CBZ) at 4,000 rpm for 25 s, followed by annealing at 100°C for 5 min. Finally, C60 (27 nm), BCP (7 nm), and Ag (140 nm) were sequentially thermally evaporated.

Device testing

The current density-voltage (*J-V*) characteristics for the fabricated solar cells were measured using a Keithley 2450 source meter under illumination from a solar simulator (Newport, Class A Oriel Sol2A) with a light intensity of 100 mW/cm^2 (confirmed with a calibrated reference solar cell from Newport, 91150V). *J-V* curves were measured under nitrogen flow with a scanning rate of 100 mV/s (voltage step of 10 mV and delay time of 200 ms). The active area was determined by the aperture shade mask (0.049 cm^2 for small-area devices) placed in front of the solar cell and was identical to the contact area. Encapsulated substrates contained 4 devices each. EQE spectra were acquired using an Oriel model QE-PV-SI instrument equipped with a national institute of standards and technology (NIST)-certified Si diode. For tandem solar cells, EQE measurements were performed in ambient air and the bias illumination from bright light-emitting diodes (LEDs) with emission peaks of 845 and 470 nm was used for the measurements of the front and back subcells, respectively. No bias voltage was applied during the EQE measurements of the tandem solar cells.

Characterization

XRD was carried out by a Rigaku Miniflex diffractometer (Cu Kα_1 radiation). TRPL measurement was conducted using an Edinburgh FS5 spectrofluorometer with a 373-nm excitation laser. The PL decay curves were fitted by a biexponential decay function. Photoluminescence (PL) mapping was carried out by using the Horiba LabRam HR Evolution. Through confocal PL, we achieved comprehensive mapping of the large area to assess the uniformity of perovskite and Al_2O_3 samples, both with and without 5-AVAI. A 473-nm laser, a 5× objective lens, and a neutral density (ND) filter (filter: 0.01%) were utilized to minimize phase separation in the spectra, acquiring each spectrum with a 0.1-s exposure time using a 600-gr/mm grating. For the KPFM measurements, the Bruker Icon was employed, using a Pt/Si-coated tip with a spring constant of 1.6 N/m and a frequency of 61 kHz. Images were processed using Nanoscope software, including flattening of all potential images and application of a low-pass filter. The scanning rates were set at 0.1 or 0.2 Hz. High-resolution SEM images were obtained using the Hitachi S8030 microscope with an accelerating voltage of 3 kV. ToF-SIMS measurements were carried out on an IONTOF M6 instrument with a primary Bi source of 30 keV and an analysis area of 50 × 50 μm^2. The transient dark current measurement for calculation of mobile ion concentration (N_o) and the electrochemical impedance spectroscopy for calculation of ionic conductivity (σ) were performed using photo-assisted impedance and optical spectrocopy (PAIOS), an all-in-one measurement equipment for photovoltaic devices and LEDs. A Nyquist plot was obtained from the impedance spectroscopy and ionic resistance was extracted from the plot using equivalent circuit fitting to determine σ. The E_A was obtained from *in situ* ionic conductivity versus temperature measurements and determined using an Arrhenius plot of log(σT) and inverse of temperature (1/T).

RESOURCE AVAILABILITY

Lead contact

Futher information and requests for resources should be directed to and will be fulfilled by the lead contact, Bin Chen (bin.chen@northwestern.edu).

Materials availability

This study did not generate new unique materials.

Data and code availability

The data that support the findings of this study are available from the lead contact upon reasonable request.

ACKNOWLEDGMENTS

This work was supported by the Trienens Institute for Sustainability and Energy at Northwestern University. This research was made possible by the US Department of Energy's Office of Energy Efficiency and Renewable Energy (EERE) under the Solar Energy Technologies Office award no. DE-EE0010502. A.S.R.B. acknowledges the support from King Abdullah University of Science and Technology (KAUST) through the Ibn Rushd Postdoctoral Fellowship Award. This work made use of the SPID, EPIC, and Keck-II facilities of Northwestern University's NUANCE Center, which has received support from the SHyNE Resource (NSF ECCS-2025633). This material is based upon work supported by the National Science Foundation under grant no. 2339233.

AUTHOR CONTRIBUTIONS

D.C., D.S., C.L., Y.L., and A.S.R.B. contributed equally. B.C. and E.H.S. supervised the project. D.C. conceived the idea and designed the experiments. D.C. and D.S. performed the main characterization. C.L. helped to optimize the photovoltaic performance of solar cells. D.C., C.L., and Y.L. measured stability performance. Y.L. and A.S.R.B. fabricated the NBG perovskite on the WBG perovskite for tandems. Y.Y. helped with materials screening and construction of the paper. D.C. and J.L. performed ToF-SIMS measurement. D.C. and D.E.K. performed initial experiments. Y.J.L. performed XRD measurement. M.L., S.P., and N.R. performed transient dark current measurements. S.M.P. and C.L. helped fabricate and optimize the photovoltaic devices. A.M. performed PLQY measurement. D.B.K., C.-H.C., and H.W. helped to optimize the ALD-SnO_2 condition. D.S. and H.S. performed XPS analysis. D.C. wrote the first draft of the paper. D.S., C.L., B.C., and E.H.S. revised and approved the paper.

DECLARATION OF INTERESTS

B.C., E.H.S., and D.C. are filing a patent based on this work.

SUPPLEMENTAL INFORMATION

Supplemental information can be found online at https://doi.org/10.1016/j.joule.2024.12.002.

Received: September 2, 2024
Revised: October 22, 2024
Accepted: December 2, 2024
Published: January 9, 2025

REFERENCES

1. Lin, R., Wang, Y., Lu, Q., Tang, B., Li, J., Gao, H., Gao, Y., Li, H., Ding, C., Wen, J., et al. (2023). All-perovskite tandem solar cells with 3D/3D bilayer perovskite heterojunction. Nature *620*, 994–1000.
2. Lin, R., Xu, J., Wei, M., Wang, Y., Qin, Z., Liu, Z., Wu, J., Xiao, K., Chen, B., Park, S.M., et al. (2022). All-perovskite tandem solar cells with improved grain surface passivation. Nature *603*, 73–78.
3. Zhu, Q., Cox, D.E., Fischer, J.E., Kniaz, K., Mcghie, A.R., and Zhou, O. (1992). Intercalation of solid C6O with iodine. Nature *355*, 712–714.
4. Penukula, S., Estrada Torrejon, R., and Rolston, N. (2023). Quantifying and Reducing Ion Migration in Metal Halide Perovskites through Control of Mobile Ions. Molecules *28*, 5026.

5. Bi, E., Song, Z., Li, C., Wu, Z., and Yan, Y. (2021). Mitigating ion migration in perovskite solar cells. J. Trends Chem. *3*, 575–588.
6. Rivkin, B., Fassl, P., Sun, Q., Taylor, A.D., Chen, Z., and Vaynzof, Y. (2018). Effect of Ion Migration-Induced Electrode Degradation on the Operational Stability of Perovskite Solar Cells. ACS Omega *3*, 10042–10047.
7. Warby, J., Zu, F., Zeiske, S., Gutierrez-Partida, E., Frohloff, L., Kahmann, S., Frohna, K., Mosconi, E., Radicchi, E., Lang, F., et al. (2022). Understanding Performance Limiting Interfacial Recombination in pin Perovskite Solar Cells. Adv. Energy Mater. *12*, 2103567.
8. Das, C., Kot, M., Hellmann, T., Wittich, C., Mankel, E., Zimmermann, I., Schmeisser, D., Khaja Nazeeruddin, M., and Jaegermann, W. (2020). Atomic Layer-Deposited Aluminum Oxide Hinders Iodide Migration and Stabilizes Perovskite Solar Cells. Cell Rep. Phys. Sci. *1*, 100112.
9. Li, T., Xu, J., Lin, R., Teale, S., Li, H., Liu, Z., Duan, C., Zhao, Q., Xiao, K., Wu, P., et al. (2023). Inorganic wide-bandgap perovskite subcells with dipole bridge for all-perovskite tandems. Nat. Energy *8*, 610–620.
10. Chen, H., Teale, S., Chen, B., Hou, Y., Grater, L., Zhu, T., Bertens, K., Park, S.M., Atapattu, H.R., Gao, Y., et al. (2022). Quantum-size-tuned heterostructures enable efficient and stable inverted perovskite solar cells. Nat. Photonics *16*, 352–358.
11. Kim, D.H., Muzzillo, C.P., Tong, J., Palmstrom, A.F., Larson, B.W., Choi, C., Harvey, S.P., Glynn, S., Whitaker, J.B., Zhang, F., et al. (2019). Bimolecular Additives Improve Wide-Band-Gap Perovskites for Efficient Tandem Solar Cells with CIGS. Joule *3*, 1734–1745.
12. Wang, S., Wang, A., Deng, X., Xie, L., Xiao, A., Li, C., Xiang, Y., Li, T., Ding, L., and Hao, F. (2020). Lewis acid/base approach for efficacious defect passivation in perovskite solar cells. J. Mater. Chem. A *8*, 12201–12225.
13. Caprioglio, P., Cruz, D.S., Caicedo-Dávila, S., Zu, F., Sutanto, A.A., Peña-Camargo, F., Kegelmann, L., Meggiolaro, D., Gregori, L., Wolff, C.M., et al. (2021). Bi-functional interfaces by poly(ionic liquid) treatment in efficient pin and nip perovskite solar cells. Energy Environ. Sci. *14*, 4508–4522.
14. Zhu, Z., Mao, K., Zhang, K., Peng, W., Zhang, J., Meng, H., Cheng, S., Li, T., Lin, H., Chen, Q., et al. (2022). Correlating the perovskite/polymer multimode reactions with deep-level traps in perovskite solar cells. Joule *6*, 2849–2868.
15. Koushik, D., Verhees, W.J.H., Kuang, Y., Veenstra, S., Zhang, D., Verheijen, M.A., Creatore, M., and Schropp, R.E.I. (2017). High-efficiency humidity-stable planar perovskite solar cells based on atomic layer architecture. Energy Environ. Sci. *10*, 91–100.
16. Dong, X., Fang, X., Lv, M., Lin, B., Zhang, S., Ding, J., and Yuan, N. (2015). Improvement of the humidity stability of organic-inorganic perovskite solar cells using ultrathin Al_2O_3 layers prepared by atomic layer deposition. J. Mater. Chem. A *3*, 5360–5367.
17. Artuk, K., Turkay, D., Mensi, M.D., Steele, J.A., Jacobs, D.A., Othman, M., Yu Chin, X., Moon, S.J., Tiwari, A.N., Hessler-Wyser, A., et al. (2024). A Universal Perovskite/C60 Interface Modification via Atomic Layer Deposited Aluminum Oxide for Perovskite Solar Cells and Perovskite–Silicon Tandems. Adv. Mater. *36*, e2311745.
18. Ji, X., Ding, Y., Bi, L., Yang, X., Wang, J., Wang, X., Liu, Y., Yan, Y., Zhu, X., Huang, J., et al. (2024). Multifunctional Buffer Layer Engineering for Efficient and Stable Wide-Bandgap Perovskite and Perovskite/Silicon Tandem Solar Cells. Angew. Chem. Int. Ed. Engl. *63*, e202407766.
19. Hultqvist, A., Jacobsson, T.J., Svanström, S., Edoff, M., Cappel, U.B., Rensmo, H., Johansson, E.M.J., Boschloo, G., and Törndahl, T. (2021). SnO_xAtomic Layer Deposition on Bare Perovskite - An Investigation of Initial Growth Dynamics, Interface Chemistry, and Solar Cell Performance. ACS Appl. Energy Mater. *4*, 510–522.
20. Ren, N., Zhu, C., Li, R., Mazumdar, S., Sun, C., Chen, B., Xu, Q., Wang, P., Shi, B., Huang, Q., et al. (2022). 50 °C low-temperature ALD SnO_2 driven by H_2O_2 for efficient perovskite and perovskite/silicon tandem solar cells. Appl. Phys. Lett. *121*, 033502.
21. Heo, J., Hock, A.S., and Gordon, R.G. (2010). Low temperature atomic layer deposition of tin oxide. Chem. Mater. *22*, 4964–4973.
22. Zhao, R., Zhang, K., Zhu, J., Xiao, S., Xiong, W., Wang, J., Liu, T., Xing, G., Wang, K., Yang, S., et al. (2021). Surface passivation of organometal halide perovskites by atomic layer deposition: An investigation of the mechanism of efficient inverted planar solar cells. Nanoscale Adv. *3*, 2305–2315.
23. Palmstrom, A.F., Raiford, J.A., Prasanna, R., Bush, K.A., Sponseller, M., Cheacharoen, R., Minichetti, M.C., Bergsman, D.S., Leijtens, T., Wang, H.P., et al. (2018). Interfacial Effects of Tin Oxide Atomic Layer Deposition in Metal Halide Perovskite Photovoltaics. Adv. Energy Mater. *8*, 1800591.
24. Gao, D., Li, R., Chen, X., Chen, C., Wang, C., Zhang, B., Li, M., Shang, X., Yu, X., Gong, S., et al. (2023). Managing Interfacial Defects and Carriers by Synergistic Modulation of Functional Groups and Spatial Conformation for High-Performance Perovskite Photovoltaics Based on Vacuum Flash Method. Adv. Mater. *35*, e2301028.
25. Jiang, Q., Zhao, Y., Zhang, X., Yang, X., Chen, Y., Chu, Z., Ye, Q., Li, X., Yin, Z., and You, J. (2019). Surface passivation of perovskite film for efficient solar cells. Nat. Photonics *13*, 460–466.
26. Hu, J., Oswald, I.W.H., Stuard, S.J., Nahid, M.M., Zhou, N., Williams, O.F., Guo, Z., Yan, L., Hu, H., Chen, Z., et al. (2019). Synthetic control over orientational degeneracy of spacer cations enhances solar cell efficiency in two-dimensional perovskites. Nat. Commun. *10*, 1276.
27. Chen, H., Maxwell, A., Li, C., Teale, S., Chen, B., Zhu, T., Ugur, E., Harrison, G., Grater, L., Wang, J., et al. (2023). Regulating surface potential maximizes voltage in all-perovskite tandems. Nature *613*, 676–681.
28. Wang, M., Shi, Z., Fei, C., Deng, Z.J.D., Yang, G., Dunfield, S.P., Fenning, D.P., and Huang, J. (2023). Ammonium cations with high pKa in perovskite solar cells for improved high-temperature photostability. Nat. Energy *8*, 1229–1239.
29. Paez-Ornelas, J.I., Fernández-Escamilla, H.N., Borbón-Nuñez, H.A., Tiznado, H., Takeuchi, N., and Guerrero-Sánchez, J. (2021). A first-principles study of the atomic layer deposition of ZnO on carboxyl functionalized carbon nanotubes: The role of water molecules. Phys. Chem. Chem. Phys. *23*, 3467–3478.
30. Choi, S., Ansari, A.S., Yun, H.J., Kim, H., Shong, B., and Choi, B.J. (2021). Growth of Al-rich AlGaN thin films by purely thermal atomic layer deposition. J. Alloys Compd. *854*, 157186.
31. Yun, H.J., Kim, H., and Choi, B.J. (2020). Nucleation and growth behavior of aluminum nitride film using thermal atomic layer deposition. Ceram. Int. *46*, 13372–13376.
32. Zhang, Y., Tao, J.J., Chen, H.Y., and Lu, H.L. (2021). Preparation of single crystalline AlN thin films on ZnO nanostructures by atomic layer deposition at low temperature. Nanotechnology *32*, 275704.
33. Li, M., Dai, M., and Chabal, Y.J. (2009). Atomic layer deposition of aluminum oxide on carboxylic acid-terminated self-assembled monolayers. Langmuir *25*, 1911–1914.
34. Liu, J., De Bastiani, M., Aydin, E., Harrison, G.T., Gao, Y., Pradhan, R.R., Eswaran, M.K., Mandal, M., Yan, W., Seitkhan, A., et al. (2022). Efficient and stable perovskite-silicon tandem solar cells through contact displacement by MgF_x. Science *377*, 302–306.
35. Xu, Z., Kerner, R.A., Harvey, S.P., Zhu, K., Berry, J.J., and Rand, B.P. (2023). Halogen Redox Shuttle Explains Voltage-Induced Halide Redistribution in Mixed-Halide Perovskite Devices. ACS Energy Lett. *8*, 513–520.